L_1 ADAPTIVE CONTROL AUGMENTATION SYSTEM FOR THE X-48B AIRCRAFT

BY

TYLER JOHN LEMAN

THESIS

Submitted in partial fulfillment of the requirements
for the degree of Master of Science in Mechanical Engineering
in the Graduate College of the
University of Illinois at Urbana-Champaign, 2009

Urbana, Illinois

Advisers:

Professor Naira Hovakimyan
Professor Geir E. Dullerud

Abstract

This thesis considers the application of $\mathcal{L}_1$ adaptive control methodology to a model of the X-48B Blended Wing Body aircraft. We explicitly verify the performance bounds of the adaptive flight control system at various flight conditions. We demonstrate that the resulting $\mathcal{L}_1$ adaptive controller does not require tuning or redesign from one flight condition to another. Furthermore, once designed according to the theoretical guidelines, the $\mathcal{L}_1$ adaptive controller ensures uniform transient and steady-state performance across the entire flight envelope in the presence of significantly coupled dynamics and control surface failures.

Acknowledgements

I would like to sincerely thank my advisers, Professor Naira Hovakimyan and Professor Geir Dullerud, for giving me the opportunity to work on this project and investing their time in my education. I also want to thank Enric Xargay, who spent many hours helping me understand $\mathcal{L}_1$ theory and implementation. Thank you to Evgeny Kharisov for his help formatting this thesis. And finally, a big thank you to Rachel and my parents for their constant support.

Contents

Chapter 1

Introduction

1.1 Background and Motivation[1]

Aircraft loss of control (LOC) during flight is a leading cause of fatal aviation accidents [2]. Loss of control can result from any number of factors, including system and component failures, control system impairment or damage, inclement weather, or inappropriate pilot inputs. In general, a loss of control accident takes the airplane beyond the normal flight envelope into regions where aerodynamic data is not available from conventional sources. For example, wind tunnel test data for aerodynamic forces and moments at high angles of attack is limited in accuracy, as is modeling the effect of a control surface failure on the aircraft's dynamics. Thus, the aerodynamic changes due to such failures cannot be predicted a priori.

[1] Much of the work contained in this thesis has been previously published in Reference [1] and is reprinted with permission.

Adaptive control is a viable technology for constructing an upset recovery system or an upset prevention system, without having such models available a priori. However, the conventional theory of adaptive control has a limited analysis framework for its transient performance and robustness guarantees. As mentioned in [3], arbitrary bad transients can occur even when the adaptive system is stable. The transient performance can change drastically with a change in adaptive gains, reference inputs, initial conditions, and values of uncertain coefficients. The highly nonlinear dependence in between these parameters, introduced via the adaptive laws, makes the theoretical analysis of transient performance and stability margins very challenging. As a result, since research in adaptive control began in the 1950's, it has largely remained a tool for adapting to slowly varying uncertainties. Fast adaptation has typically led to high frequency oscillations and reduced the system's tolerance to time delay. Fast adaptation is critical, however, because in the seconds following a failure the aircraft may leave the portion of the flight envelope where the pilot is trained to fly.

The previously mentioned nonlinearities in the adaptive system also make the certification process for adaptive flight control very challenging. The notion of a phase margin for a nonlinear system is not defined, thus determining the robustness of a system requires use of the time delay margin, the extension of phase margin for nonlinear systems. For traditional adaptive controllers, verifying the time delay margin is a lengthy process requiring a large number of Monte Carlo simulations. The number of Monte Carlo sim-

ulations required also increases with the increasing complexity of the flight control system (FCS). This fact combined with the criticality of inner-loop control leads to high certification costs. Thus implementing traditional adaptive control typically increases the complexity of the flight control system beyond the capability of current Verification and Validation (V&V) processes.

1.2 $\mathcal{L}_1$ Adaptive Control Overview

The $\mathcal{L}_1$ adaptive control methodology addresses the problems of traditional adaptive control by providing fast and robust adaptation, which leads to desired transient performance for the systems input and output signals simultaneously, in addition to steady-state tracking. It also provides guaranteed, analytically provable, bounded away from zero, time delay margin [4–6]. The decoupling between fast adaptation and robustness, inherent to all $\mathcal{L}_1$ adaptive control architectures, is achieved via the introduction of a low-pass filter on the adaptive control signal. This filter is introduced with the understanding that uncertainties in any feedback loop can only be compensated for within the bandwidth of the control channel.

$\mathcal{L}_1$ adaptive control theory's systematic design procedures also significantly reduce the tuning effort required to achieve desired closed-loop performance, particularly while operating in the presence of uncertainties and failures. Its fast adaptation ability allows for control of time-varying nonlinear systems by adapting two parameters only, the adaptive gain and filter

bandwidth [7]. The theory shifts the tuning issue from the selection of the adaptive gain for a *nonlinear* gradient minimization algorithm to determining the structure/bandwidth for a *linear* low-pass filter in the feedback path.

The main features of the $\mathcal{L}_1$ adaptive control methodology are summarized below:

1. Decoupling between the rate of adaptation and robustness;
2. Guaranteed fast adaptation, limited only by hardware constraints;
3. Guaranteed transient performance for a system's input and output signals, without high gain feedback or enforcing persistent excitation type assumptions;
4. Guaranteed, bounded away from zero time delay margin;
5. Uniform, scaled transient response dependent on changes in initial conditions, unknown parameters, and reference commands.

Thus, $\mathcal{L}_1$ theory has the potential to reduce V&V costs for adaptive control. Because $\mathcal{L}_1$ provides a theoretical guarantee for the time delay margin, fewer Monte Carlo simulations are required to verify robustness. The time delay margin only needs to be verified in the neighborhood of the theoretical prediction. This guarantee on the time delay margin depends on the particular system structure under consideration, as well as the type of filter being used.

The $\mathcal{L}_1$ adaptive control architecture and its variants have been verified for a number of systems: flight tests of augmentation of an off-the-shelf autopilot for path following [8, 9], autopilot design and flight test for Micro Air Vehicles (MAV) [10], tailless unstable military aircraft [11], Aerial Refueling Autopilot design [12, 13], flexible aircraft (Sensorcraft) [14], control of wingrock in the presence of faults [15], air-breathing hypersonic vehicles [16], and the NASA AirSTAR Generic Transport Model [17].

1.3 X-48B Blended Wing Body

The X-48B Blended Wing Body is an experimental aircraft being developed under NASA's Fundamental Aeronautics Program Subsonic Fixed-Wing Project, in collaboration with the Boeing Co. and the Air Force Research Laboratory (AFRL). The blended wing body concept is a cross between a conventional plane and a flying wing design. This advanced wing design and a wide airfoil-shaped body combine to generate higher lift-to-drag ratios than those found in conventional aircraft, which improves fuel economy. The blended wing body also has the potential to provide a greatly reduced noise footprint and a larger payload volume than contemporary aircraft of comparable size [18]. Thus, the X-48B has significant potential for both civilian and military applications. The X-48B is remotely piloted and is currently being flight tested at NASAs Dryden Flight Research Center. The next iteration of the aircraft, the X-48C, is currently undergoing wind-tunnel

testing.

"Certification Techniques of Advanced Flight Critical Systems Challenge Problem Integration" is a Wright-Patterson AFRL program to analyze the deficiencies of current V&V practices and advance airworthiness certification of new technologies, including adaptive flight control systems. Under this program, the Boeing Co. and the University of Illinois developed and evaluated an $\mathcal{L}_1$ adaptive inner-loop control augmentation on a model of the X-48B. The purpose of this project was to demonstrate the advantages of $\mathcal{L}_1$ adaptive control for reducing flight control design costs by providing the proper framework for V&V.

1.4 Organization of Thesis

This thesis presents an implementation of a recently developed $\mathcal{L}_1$ adaptive control augmentation system (CAS) on the X-48B aircraft at different flight conditions. Chapter 2 formulates the control problem, introduces the $\mathcal{L}_1$ adaptive controller for unmatched uncertainties, and presents the proposed $\mathcal{L}_1$ adaptive control augmentation system. Chapter 3 presents simulation results, which demonstrate the benefits of the developed adaptive control scheme. Finally, Chapter 4 summarizes the key results and presents opportunities for future work.

Chapter 2

Theoretical Framework

2.1 Baseline Control Architecture

The X-48B is equipped with a gain-scheduled baseline controller based on dynamic inversion, designed by Boeing to achieve desired performance across the flight envelope. Dynamic inversion (also known as feedback linearization) is a technique used to transform a nonlinear system into an equivalent linear system. It has been widely studied over the past 30 years and has been applied in a variety of settings, including flight control. Because any aircraft model is an imperfect representation of the actual flight dynamics, an adaptive controller can be used to augment the baseline controller and compensate for the inversion error. Here, for the first time, $\mathcal{L}_1$ adaptive control theory is applied to augment a dynamic inversion control law.

The objective of the adaptive augmentation is to compensate for the ef-

fects of control surface failures and aircraft damage, and to guarantee safe recovery of the aircraft by ensuring that it does not escape out of the operational flight envelope where pilots are trained to fly. Furthermore, adaptation can compensate for the undesirable effects of dynamic inversion errors, which might become severe in the case of an impaired aircraft.

The baseline controller developed by Boeing for the X-48B aircraft consists of a three axis angle of attack (AOA or α), roll rate (p), and sideslip angle (β) control augmentation system and is designed to yield consistent nominal system performance. This baseline controller generates virtual roll, pitch, and yaw acceleration commands ($\dot{p}_{\text{cmd}}$, $\dot{q}_{\text{cmd}}$, $\dot{r}_{\text{cmd}}$), which are then "deaugmented", yielding moment commands L_{cmd}, M_{cmd}, and N_{cmd}, for which control effort is mixed to the control surfaces accordingly. The adaptive element uses the feedback signals and the reference commands for α, p, and β to augment the control signals $\dot{p}_{\text{cmd}}$, $\dot{q}_{\text{cmd}}$, and $\dot{r}_{\text{cmd}}$ generated by the baseline controller. Figure 2.1 presents the complete inner-loop FCS using dynamic inversion with the $\mathcal{L}_1$ adaptive augmentation.

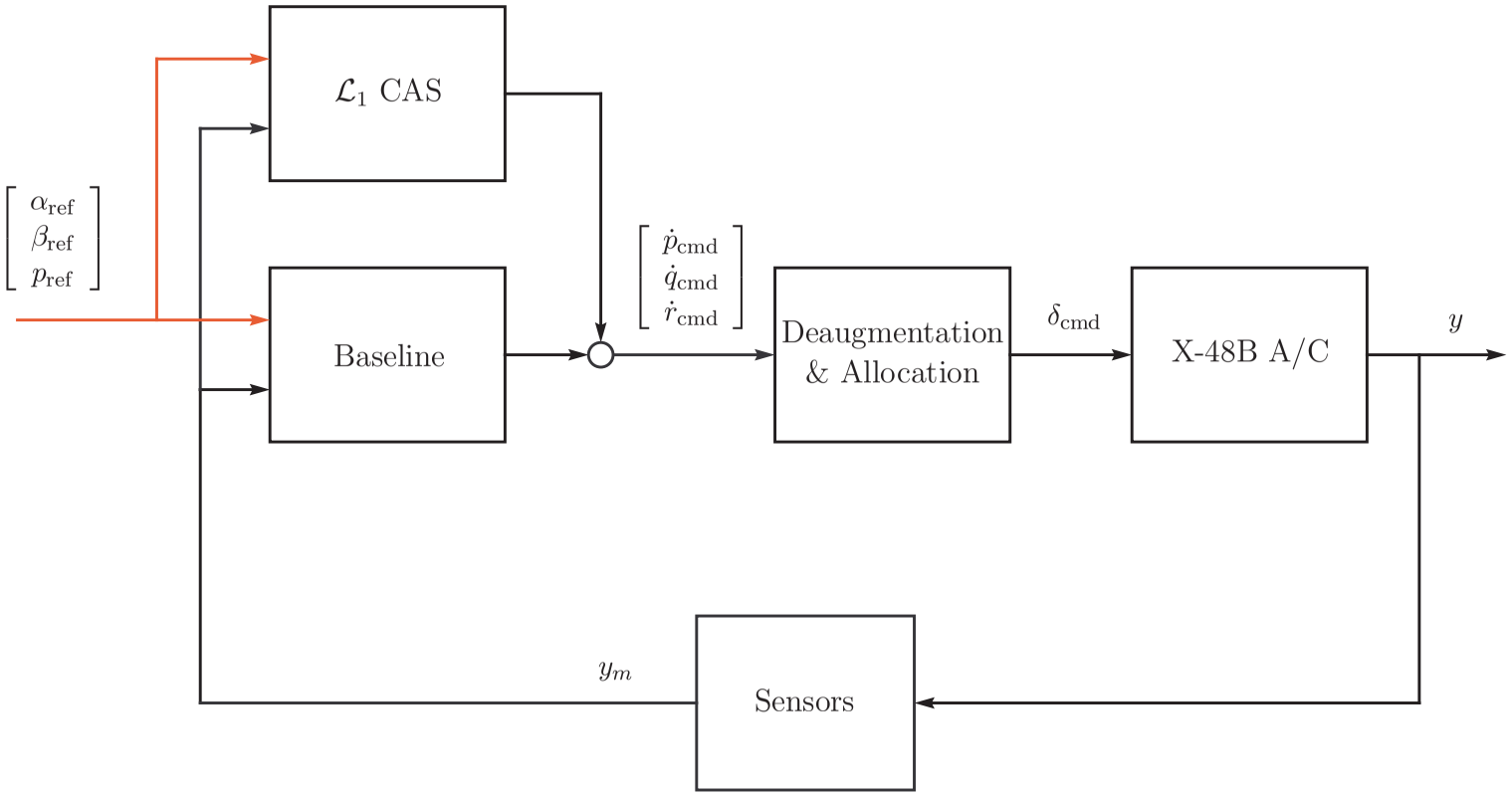

Figure 2.1: Overall Structure with $\mathcal{L}_1$ Adaptive Control

2.2 Problem Formulation

A theoretical extension of the $\mathcal{L}_1$ adaptive control theory that compensates for both *matched* as well as *unmatched* dynamic uncertainties was implemented on the X-48B model. If uncertainty is unmatched, that simply means that the uncertainty lies outside the span of a particular linear system's 'B' matrix. For inner-loop FCS design, the effects of slow outer-loop variables (e.g. airspeed, pitch angle, bank angle) may appear as unmatched uncertainties in the dynamics of the fast inner-loop variables we are trying to regulate (e.g. angle of attack, sideslip angle, roll rate). Also, unmodeled nonlinearities, cross-coupling between channels, and dynamic asymmetries may introduce unmatched uncertainties in the inner-loop system dynamics. If the design of the inner-loop FCS does not account for these uncertainties, their effect on the inner-loop dynamics will require continuous compensation by the pilot, thereby increasing the pilot's workload. Therefore, automatic compensation for the undesirable effects of these unmatched uncertainties on the output of the system is critical to achieve desired performance and improve the aircraft's handling qualities.

Next we present the theoretical framework for the development of the $\mathcal{L}_1$ adaptive augmentation system that compensates for the effects of unmatched uncertainties on the output of the system. The inner-loop dynamics

of the X-48B with the baseline controller can be written as:

$$\begin{aligned}
\dot{x}(t) &= A_m x(t) \;+\; B_1 \left(K_g r(t) + u_{ad}(t) + f_1(x(t), z(t), t)\right) \\
&\quad +\; B_2 f_2(x(t), z(t), t)\,, \quad x(0) = x_0\,, \\
z(t) &= g_o\left(x_z(t), t\right)\,, \\
\dot{x}_z(t) &= g\left(x_z(t), x(t), t\right)\,, \quad x_z(0) = x_{z0}\,, \\
y(t) &= Cx(t)\,,
\end{aligned} \tag{2.1}$$

where $x(t) \in \mathbb{R}^n$ is the system state vector (measured); $u_{ad}(t) \in \mathbb{R}^m$ is the adaptive control signal; $y(t) \in \mathbb{R}^m$ is the regulated output; A_m is a known Hurwitz $n \times n$ matrix that defines the desired dynamics for the closed-loop system; $B_1 \in \mathbb{R}^{n\times m}$ is a known constant matrix; $B_2 \in \mathbb{R}^{n\times(n-m)}$ is a constant matrix such that $B_1^\top B_2 = 0$ and $\text{rank}([B_1 \;\; B_2]) = n$; $C \in \mathbb{R}^{m\times n}$ is a known constant matrix; $K_g \in \mathbb{R}^{m\times m}$ is the baseline feedforward gain matrix; $r(t) \in \mathbb{R}^m$ is the reference signal; $z(t)$ and $x_z(t)$ are the output and the state vector of internal unmodeled dynamics; $f_1(\cdot)$, $f_2(\cdot)$, $g_o(\cdot)$, and $g(\cdot)$ are unknown nonlinear functions. In this problem formulation, $f_1(\cdot)$ represents the matched component of the uncertainties, whereas the term $B_2 f_2(\cdot)$ represents the unmatched component.

The above defined system needs to verify the following assumptions:

Assumption 1 *[Stability of internal dynamics] The z-dynamics are bounded-input-bounded-output (BIBO) stable, i.e. there exist $L_{z1} > 0$ and $L_{z2} > 0$*

such that

$$\|z_t\|_{\mathcal{L}_\infty} \;=\; L_{z1}\,\|x_t\|_{\mathcal{L}_\infty} \;+\; L_{z2}\,.$$

Further, let $X(t) \triangleq \begin{bmatrix} x^\top(t) & z^\top(t) \end{bmatrix}^\top$.

Assumption 2 *[Semiglobal Lipschitz condition] For any $\delta > 0$, there exist positive K_δ and B such that*

$$\begin{aligned} |f_j(X_1,t) - f_j(X_2,t)| &\le K_\delta\,\|X_1(t) - X_2(t)\|_\infty\,, \\ |f_j(0,t)| &\le B\,, \qquad\qquad j = 1,2 \end{aligned}$$

for all $\|X_i(t)\|_\infty \le \delta$, $i = 1,2$, uniformly in t.

Assumption 3 *[Semiglobal uniform boundedness of partial derivatives] For any $\delta > 0$, there exist $d_{f_x}(\delta) > 0$, and $d_{f_t}(\delta) > 0$ such that for any $\|x(t)\|_\infty \le \delta$, the partial derivatives of $f_j(X,t)$, $j = 1,2$, are piecewise continuous and bounded*

$$\left\|\frac{\partial f_j(X,t)}{\partial X}\right\| \;\le\; d_{f_x}(\delta)\,, \quad \left|\frac{\partial f_j(X,t)}{\partial t}\right| \;\le\; d_{f_t}(\delta)\,, \qquad j = 1,2\,.$$

Assumption 4 *[Stability of matched zero dynamics] The transmission zeros of the transfer matrix from the control input $u(t)$ to the output of the system $y(t)$, $H_1(s) = C\,(s\mathbb{I} - A_m)^{-1}\,B_1$, lie on the open left-half plane.*

With the above formulation, the desired dynamics for the closed-loop system are given by:

$$\begin{aligned} \dot{x}_m(t) &= A_m x_m(t) \; + \; B_1 K_g r(t)\,, \quad x(0) = x_0\,, \\ y_m(t) &= C x(t)\,. \end{aligned} \tag{2.2}$$

In particular, if the baseline feedforward gain K_g is chosen to be $K_g = -\left(CA_m^{-1}B_1\right)^{-1}$, then the diagonal elements of the transfer matrix $M(s) = C\left(s\mathbb{I} - A_m\right)^{-1} B_1 K_g$ have DC gain equal to one, while the off-diagonal elements have zero DC gain.

The control objective is to design an adaptive state feedback control law $u_{ad}(t)$ to compensate for the effect of both the matched and unmatched uncertainties on the output of the system $y(t)$, and ensure that $y(t)$ tracks the output response of the *desired system* $y_m(t)$ to a given bounded reference signal $r(t)$ *both in transient and steady-state*, while all other signals remain bounded.

2.3 $\mathcal{L}_1$ Adaptive Controller Formulation

Similar to previous $\mathcal{L}_1$ adaptive controllers, the philosophy of the $\mathcal{L}_1$ adaptive state feedback controller for unmatched uncertainties is to obtain an estimate of the uncertainties and define a control signal which compensates for the effect of these uncertainties on the output $y(t)$ within the bandwidth of low-pass filters introduced in the feedback loop. These filters guarantee that the

$\mathcal{L}_1$ adaptive controller stays in the low-frequency range even in the presence of fast adaptation and large reference inputs. The choice of the low-pass filters leads to separation between performance and robustness. Adaptation is based on a piecewise constant adaptive law and uses the output of a state predictor to update the estimate of the uncertainties.

The elements of $\mathcal{L}_1$ adaptive controller are introduced below.

State Predictor:

$$\begin{aligned} \dot{\hat{x}}(t) &= A_m\hat{x}(t) \;+\; B_1K_gr(t) \;+\; B_1\left(u_{ad}(t)+\hat{\sigma}_1(t)\right) \;+\; B_2\hat{\sigma}_2(t) \\ \hat{x}(0) &= x_0 \\ \hat{y}(t) &= C\hat{x}(t) \end{aligned} \tag{2.3}$$

The state predictor replicates the closed-loop system structure, with the estimates $\hat{\sigma}_1(t)$ and $\hat{\sigma}_2(t)$ replacing the unknown parameters and using the adaptive control signal $u_{ad}(t)$ defined below.

Adaptive Laws:

The adaptive parameters are governed by the following piecewise constant adaptive law:

$$\hat{\sigma}_1(t) = \hat{\sigma}_1(kT_s)\,, \quad \hat{\sigma}_2(t) = \hat{\sigma}_2(kT_s)\,, \quad t \in [kT_s, (k+1)T_s]$$

$$\begin{bmatrix} \hat{\sigma}_1(kT_s) \\ \hat{\sigma}_2(kT_s) \end{bmatrix} = -\begin{bmatrix} B_1 & B_2 \end{bmatrix}^{-1} \Phi^{-1}(T_s)\mathrm{e}^{A_m T_s}\tilde{x}(kT_s) \qquad (2.4)$$

$k = 0, 1, 2, ...$

where T_s is the sampling rate of the model, $\Phi(T_s) = A_m^{-1}\left(\mathrm{e}^{A_m T_s} - \mathbb{I}\right)$, and $\tilde{x}(t) = \hat{x}(t) - x(t)$ is updated every T_s.

Control Law:

$$u_{ad}(s) = -\underbrace{C_1(s)\hat{\sigma}_1(s)}_{u_{\mathrm{ad}_1}} - \underbrace{C_2(s)H_1^{-1}(s)H_2(s)\hat{\sigma}_2(s)}_{u_{\mathrm{ad}_2}} \qquad (2.5)$$

where

$$H_1(s) = C_m\left(s\mathbb{I} - A_m\right)^{-1}B_1\,, \quad H_2(s) = C_m\left(s\mathbb{I} - A_m\right)^{-1}B_2\,.$$

$C_1(s)$ is a strictly proper stable filter and $C_2(s)$ is selected to ensure that $C_2(s)H_1^{-1}(s)H_2(s)$ is also proper and stable. Furthermore, the transmission zeros of $H_1(s)$ need to lie on the open left-half plane. Regarding the structure of u_{ad_2}, note that $H_2(s)\hat{\sigma}_2(s)$ is the estimated effect of the unmatched uncertainties on the output of the plant, while $-H_1^{-1}(s)H_2(s)\hat{\sigma}_2(s)$ would be the control signal needed to cancel this effect. The low-pass filters $C_1(s)$ and $C_2(s)$ serve to attenuate high frequencies in the adaptive control signals,

and thus define the performance-robustness trade-off. By designing a filter with a lower cutoff frequency, the robustness of the adaptive controller can be systematically tuned to increase the time delay margin. Similarly a filter with a higher cutoff frequency will exhibit improved performance, at the cost of a reduced time delay margin. The proof of the performance bounds of this architecture can be found in Ref. [19]

Although the $\mathcal{L}_1$ adaptive controller does not require gain scheduling, it can be used to augment a gain scheduled baseline controller, as is the case for the X-48B. Thus, one can specify varying desired performance specifications across the flight envelope without changing the adaptive portion of the controller. Also, the rate of adaptation is decoupled from the robustness of the controller. and limited only by hardware (or simulation step time) constraints. The trade-off between performance and robustness is determined by the low-pass filters on the adaptive control signals, not by an adaptive gain. By decreasing the bandwidth of this filter, robustness can be improved with reduced performance, and vice versa.

The reader will find in Ref. [17] an application of this same extension of the $\mathcal{L}_1$ adaptive control theory to the design of an inner-loop FCS for the NASA Airborne Subscale Transport Aircraft Research (AirSTAR) system. The main difference between these two designs is that, while in this paper we use the $\mathcal{L}_1$ adaptive controller as an augmentation system, we consider a full adaptive FCS without a baseline controller for the the AirSTAR.

Chapter 3

Simulation Results

3.1 Remarks on the Implementation

High-fidelity, six degree of freedom linear Simulink models of the X-48B were provided by Boeing for a wide range of flight conditions, up to post stall angle of attack and maximum sideslip. The $\mathcal{L}_1$ adaptive controller was then implemented in Simulink to augment the baseline longitudinal, lateral, and directional control laws. The simulation contained the baseline X-48B inner-loop control laws, sensor processing and filtering, as well as actuator dynamics. The baseline control laws of the X-48B model were not modified, and the entire controller (including the $\mathcal{L}_1$ adaptive controller) was simulated at the original sampling rate of 200 Hz. Here $\mathcal{L}_1$ adaptive controller was designed strictly for pilot-in-the-loop flying, hence there is no outer-loop compensation to hold altitude, speed, or bank angle. A single-input single-

output $\mathcal{L}_1$ adaptive controller was added to each of the three control channels (Figure 3.1). The adaptive control architecture for each channel was exactly the same, consisting of the control law, state predictor, and adaptive law. These are the three basic components required for any implementation of an $\mathcal{L}_1$ adaptive control system.

Using this SISO structure, the $\mathcal{L}_1$ controller in the longitudinal channel augmented the pitch acceleration command generated by the baseline controller to achieve the desired longitudinal dynamics specified by the state predictor. Likewise, the lateral and directional channels independently augmented the baseline roll and yaw acceleration commands, respectively. The state predictor for each channel was constructed to mimic a transfer function specifying that channel's desired dynamics. These desired dynamics were second-order for the longitudinal and directional channels and first-order for the roll response.

At each flight condition, the state predictor matrices A_m, B_1, and B_2 were recomputed using the provided state space models of the control input deaugmentation, allocation, and aircraft response (Figure 2.1). A vector of state feedback gains was used with the system matrix B_1 to place the state predictor poles at the locations specified by the desired dynamics transfer functions. A_m is the matrix resulting from this pole placement. The matrix B_2 is straightforwardly computed to satisfy the conditions $B_1^\top B_2 = 0$ and $\text{rank}([B_1\ B_2]) = n$ as specified in Section 2.2. Thus the state predictor matrices A_m and B_1 ultimately represent the desired, decoupled dynamics with

either $\dot{p}_{des}$, $\dot{q}_{des}$, or $\dot{r}_{des}$ as the input, depending on the channel, while B_2 ultimately allows the adaptive controller to compensate for uncertainty outside the span of B_1. It is important to note that the input to the state predictor must always be the same as the control input that is being augmented, in this case the acceleration commands.

Finally, the low-pass filters $C_1(s)$ and $C_2(s)$, for the matched and unmatched uncertainty channels respectively, are chosen as first-order filters and their bandwidth is adjusted based on the desired trade-off between performance and robustness.

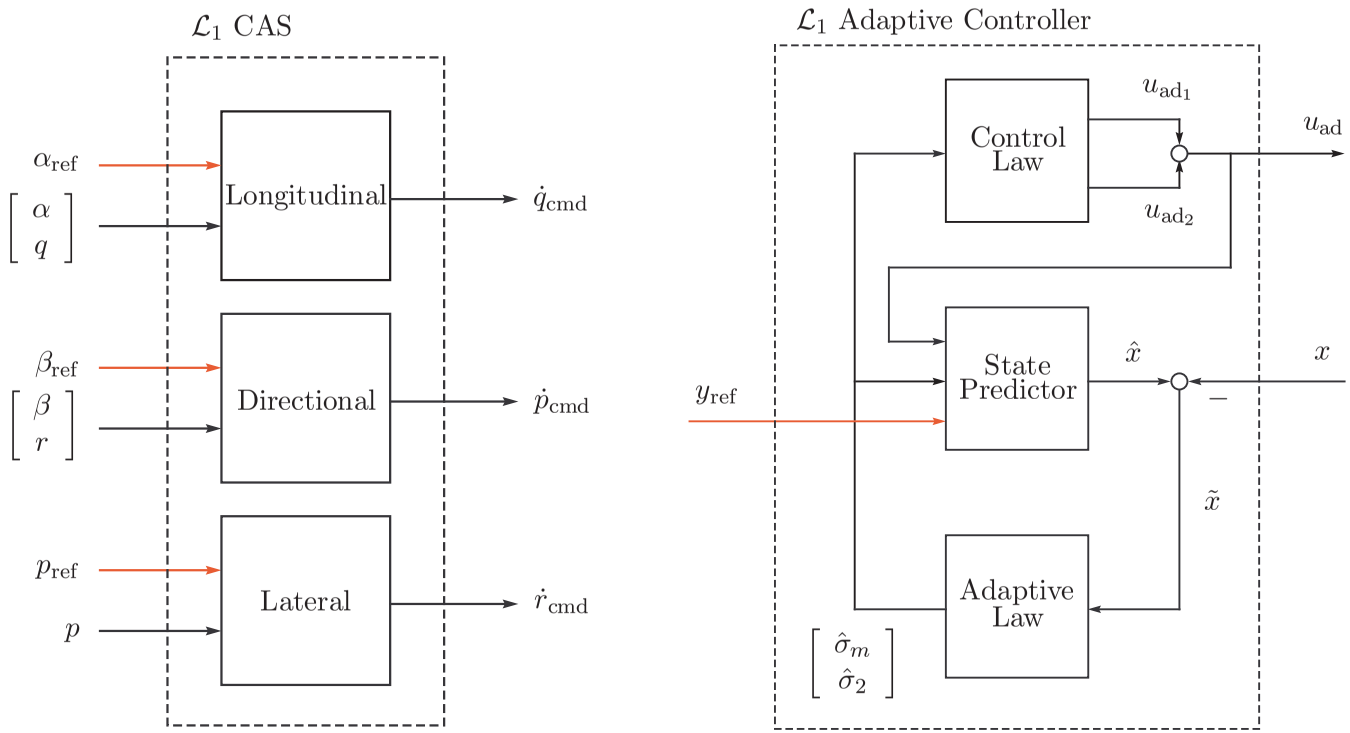

(a) $\mathcal{L}_1$ CAS Architecture

(b) $\mathcal{L}_1$ Controller Structure

Figure 3.1: $\mathcal{L}_1$ Adaptive Control Augmentation System

3.2 Results at Stall AOA Trim

Adding the $\mathcal{L}_1$ adaptive controller greatly improved angle of attack, sideslip, and roll rate command tracking, particularly at high angles of attack. The following plots represent deviations from the trim conditions. Small reference commands were used because the models were derived from linearizations at a particular flight condition. Figure 3.2a shows the angle of attack tracking performance for a pitch doublet at stall angle of attack trim. One can see from Figures 3.2b and 3.2c that there is strong coupling between the longitudinal and lateral/directional dynamics, due primarily to nonzero sideslip trim. The pitch command leads to large changes in sideslip and roll rate. However, with the $\mathcal{L}_1$ adaptive controller, the aircraft maintains sideslip and roll rate significantly closer to trim conditions than with the baseline controller alone. We also note that the $\mathcal{L}_1$ adaptive controller does not lead to high frequencies in the control surface deflections (Figure 3.2d).

The $\mathcal{L}_1$ adaptive augmentation also maintains improved performance in the event of control surface failures. Performance is recovered without the use of failure detection and isolation methods. Figure 3.3 shows the angle of attack tracking performance of the baseline controller versus its performance with the $\mathcal{L}_1$ adaptive controller with a symmetric 80% loss of control effectiveness in the inboard elevons, representing half of the total number of control surfaces. The $\mathcal{L}_1$ adaptive controller did not require any retuning or reconfiguration from the nominal case to compensate for this failure. When

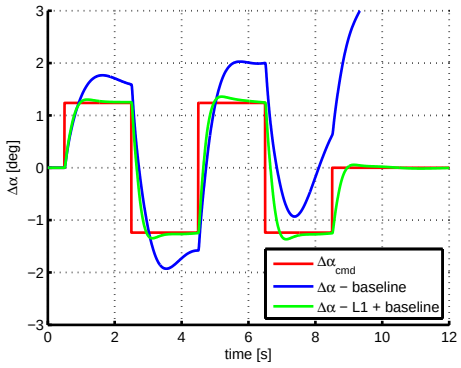

(a) Angle of Attack

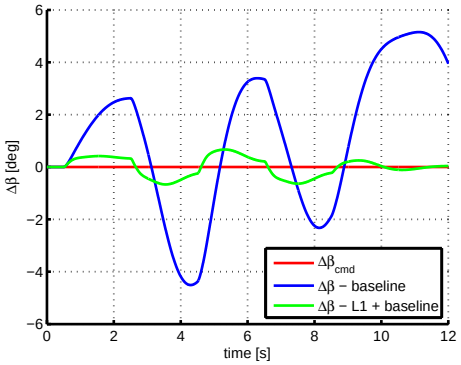

(b) Sideslip

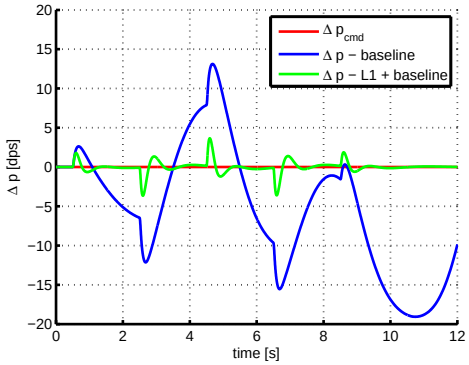

(c) Roll Rate

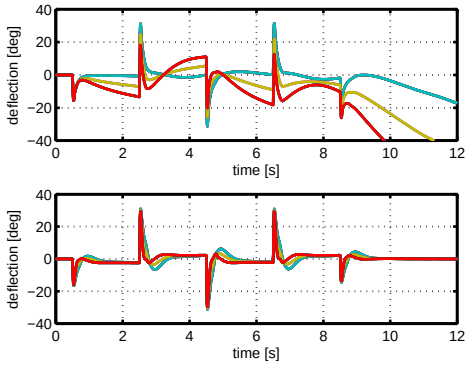

(d) Control Surface Deflections with Baseline Controller (Top) and with $\mathcal{L}_1$ CAS (Bottom)

Figure 3.2: Pitch Command at Stall AOA Trim

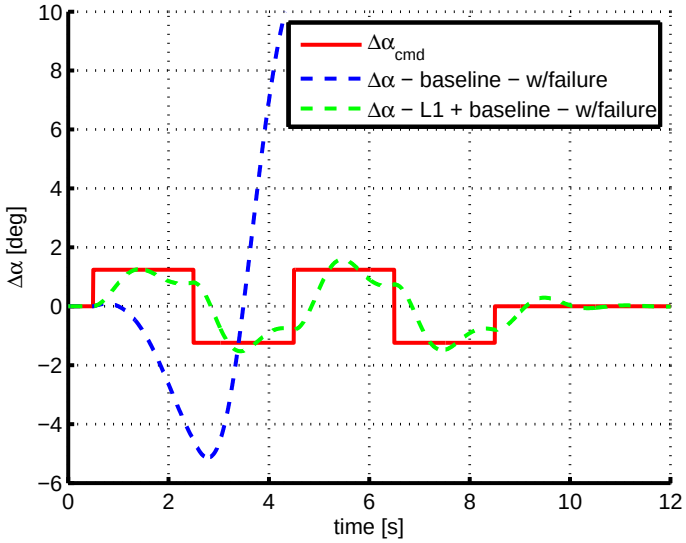

Figure 3.3: AOA Tracking at Stall AOA Trim, with Failure

the failure is introduced, the tracking performance with $\mathcal{L}_1$ augmentation exhibits a slower transient response with increased oscillation, but the aircraft generally tracks the reference command. Without $\mathcal{L}_1$ augmentation, the baseline controller is incapable of tracking the reference command and the system becomes unstable.

3.3 Results at Normal Flight AOA Trim

The same design, without any retuning, was applied for flight conditions at low angles of attack. Specifically, "without any retuning" means that the sampling time of the adaptive laws and the design of the filter remained the same. The benefits of $\mathcal{L}_1$ adaptive augmentation are shown here for a normal

flight angle of attack trim condition. Again, small reference commands were used because the given models are linearized about a single flight condition. With a symmetric 80% loss of control effectiveness in the inboard elevons the $\mathcal{L}_1$ augmented baseline controller enables the aircraft to nearly recover the nominal performance (Figure 3.4a). Figures 3.4b and 3.4c show that the $\mathcal{L}_1$ augmentation does not lead to undesirable behavior in the directional and lateral dynamics. The $\mathcal{L}_1$ augmentation also eliminates the steady state error in the roll rate tracking, in the absence any control surface failures (Figure 3.5c). Figures 3.5a and 3.5b again show that the $\mathcal{L}_1$ augmentation does not produce undesirable behavior in the longitudinal or directional dynamics. Note that the α_{cmd} in Figure 3.5a is not commanded directly. Rather, it arises in response to additional logic based on the aircraft's response to the roll rate command.

In addition to the 80% loss of control effectiveness, the case of 200% control effectiveness, corresponding to increasing the loop gain by a factor of two, was checked to ensure at least a 6 dB gain margin. As Figure 3.9 shows, the $\mathcal{L}_1$ adaptive controller remains stable given this increase in control effectiveness, and in fact reduces the amount of overshoot exhibited by the baseline controller alone. Again, the controller was in no way retuned or redesigned to compensate for this failure, which highlights the fact that the $\mathcal{L}_1$ control augmentation system does not require changes to the filter design or rate of adaptation for unpredictable changes in a system's dynamics.

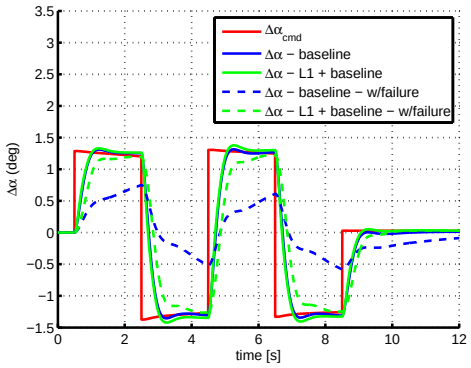

(a) Angle of Attack

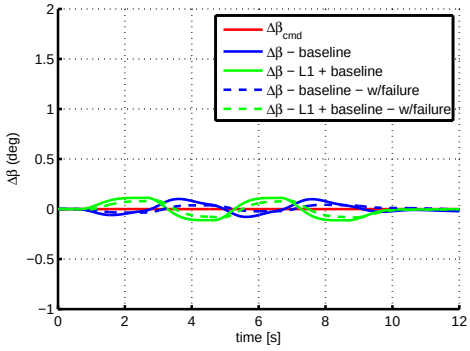

(b) Sideslip

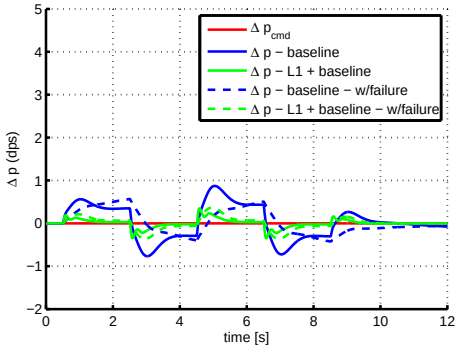

(c) Roll Rate

Figure 3.4: Pitch Command at Normal Flight AOA Trim

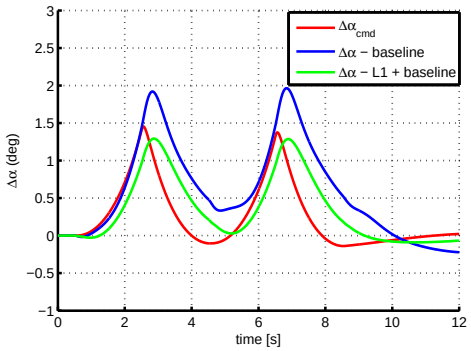

(a) Angle of Attack

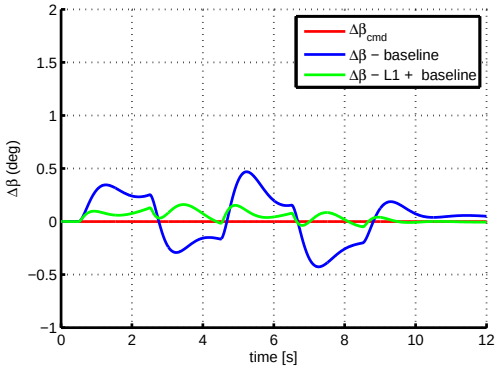

(b) Sideslip

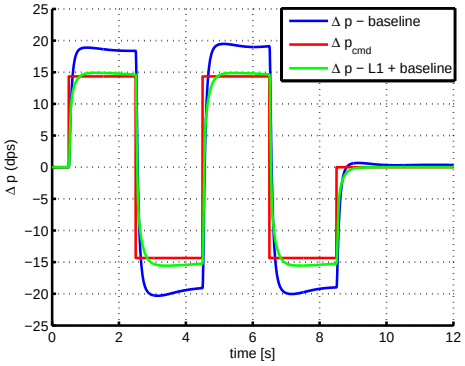

(c) Roll Rate

Figure 3.5: Roll Rate Command at Normal Flight AOA Trim

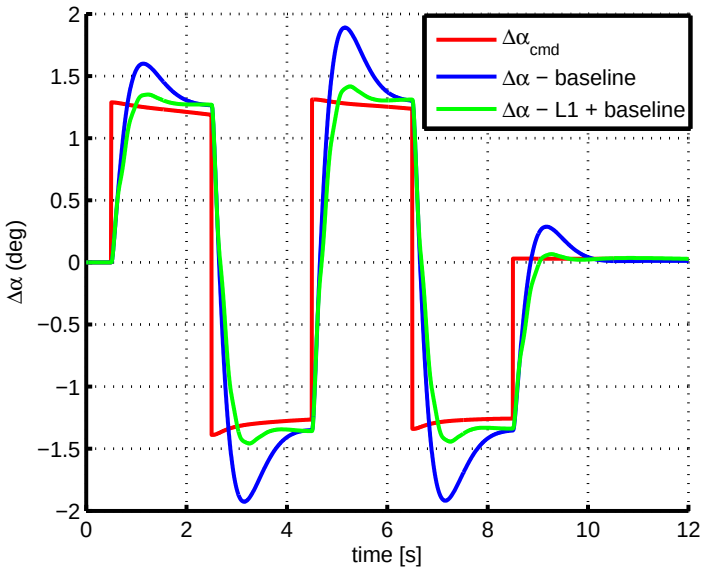

Figure 3.6: AOA Tracking with 200% Control Effectiveness

3.4 Time Delay Margin

For the above examples, the adaptive control signal passes through a first order filter. By reducing the bandwidth of the filter, and thus attenuating more of the adaptive control signal, the time delay margin of the system can be systematically increased at the cost of reduced performance. Likewise, by increasing the bandwidth of the filter the performance of adaptive closed-loop system can be arbitrarily improved, at the cost of reduced robustness. Table 3.1 summarizes the time delay margins for simulations at the two angle of attack trim conditions previously described, using various bandwidths (ω) for a first-order filter on the adaptive control signal. We determined these margins by seeing how much time delay the system could tolerate at its input before becoming marginally stable. The time delay margins were checked both with and without an asymmetric loss of control effectiveness, which affected all three control channels. The margins given below are in addition to any time delay that is already modeled in the X-48B simulation. These results are slightly improved from those in [1] due to the addition of actuator dynamics in the state predictor.

To demonstrate this performance/robustness trade-off, the time delay margin was increased from 50 ms to 135 ms for the "no failure" condition at normal flight angle of attack trim, at the expense of some performance. To achieve these improved time delay margins, a first order filter with a bandwidth of 4 rad/s was used, compared with 15 rad/s in Figures 3.4 and 3.5.

By comparing Figures 3.7 and 3.8 with Figures 3.4a and 3.5c, one can observe the trade-off in performance to achieve improved time delay margin for this example. Likewise, the time delay margin for the "no failure" condition at stall angle of attack trim was increased from 30 ms to 100 ms. For this case the trade-off between performance and robustness can be seen by comparing Figure 3.9 with Figure 3.2a. Figure 3.10 shows that we are still able to compensate for failures at stall angles of attack, even with the reduced bandwidth filter. This figure can be compared with Figure 3.3.

Thus, the performance-robustness trade-off for the $\mathcal{L}_1$ adaptive controller can be reduced to the selection of the bandwidth of a first-order filter. LMI techniques can also be utilized to determine an optimal filter structure (not necessarily first-order) that maximizes the time delay margin for the given desired performance level [20]. Further detailed analysis of the performance/robustness trade-off in terms of filter optimization is not pursued in this thesis.

AOA Trim	**Failure**	**Baseline margin**	$\mathcal{L}_1$ **+ Baseline margin**		
			$\omega = 15$	$\omega = 8$	$\omega = 4$
Normal	None	250ms	50ms	85ms	135ms
Normal	Asym. 80% LOC	350ms	70ms	105ms	155ms
Stall	None	160ms	30ms	50ms	100ms
Stall	Asym. 80% LOC	No performance	55ms	80ms	125ms

Table 3.1: Time Delay Margin Comparison

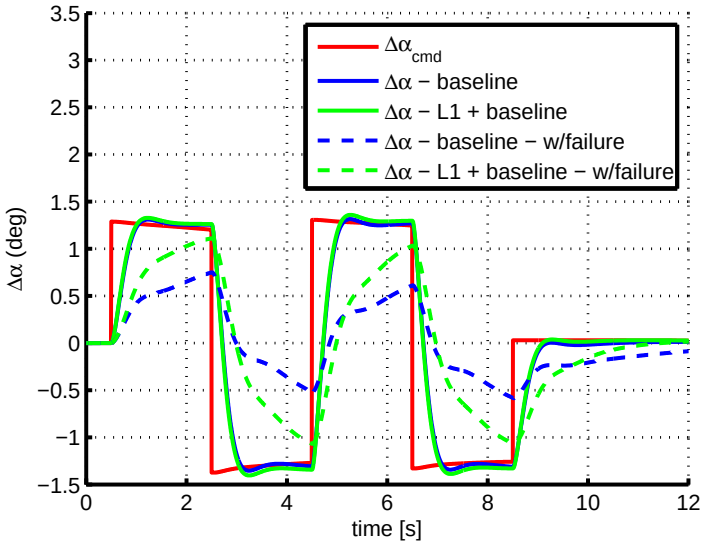

Figure 3.7: AOA Tracking with Reduced Bandwidth Filter at Normal Flight AOA Trim

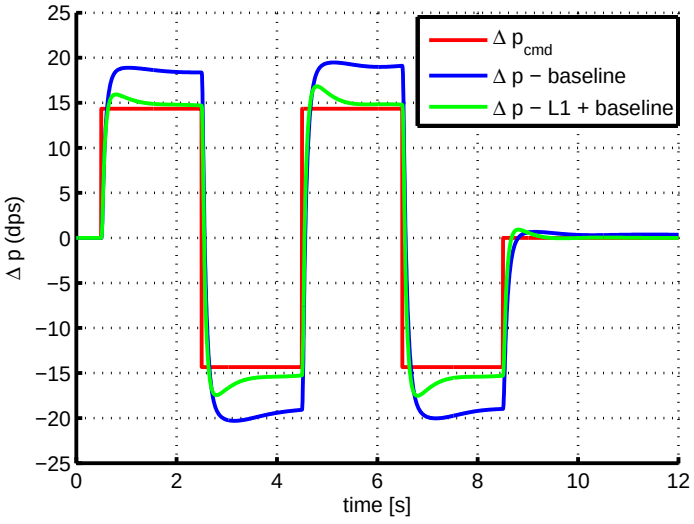

Figure 3.8: Roll Rate Tracking with Reduced Bandwidth Filter at Normal Flight AOA Trim

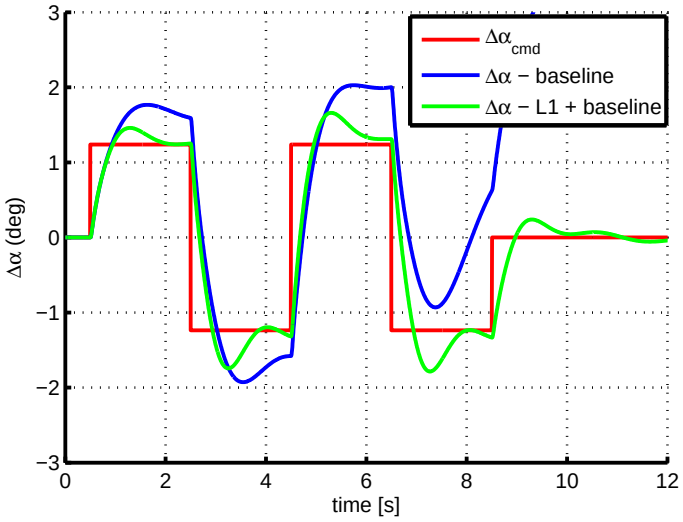

Figure 3.9: AOA Tracking with Reduced Bandwidth Filter at Stall AOA Trim

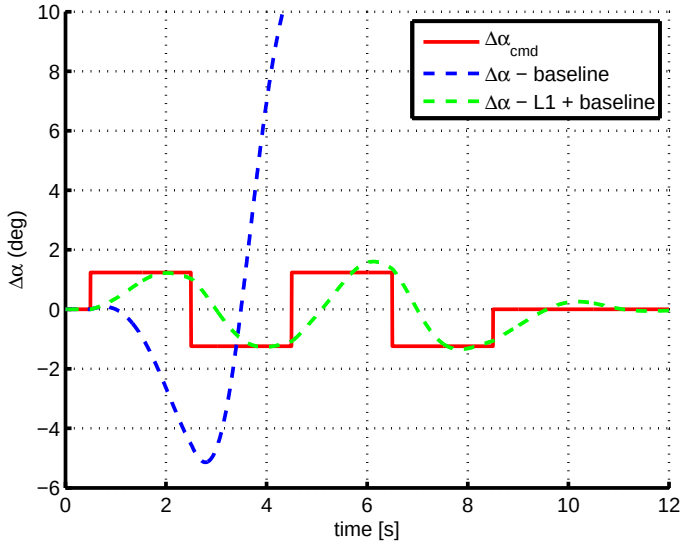

Figure 3.10: AOA Tracking with Reduced Bandwidth Filter at Stall AOA Trim with Failure

3.5 Comparison of Virtual Control Commands

Finally, we verified that the low-pass filters in the control law ensure that the virtual roll, pitch, and yaw commands are in the low frequency range. The filters can be straightforwardly designed to achieve comparable adaptive control signal amplitudes and rates with respect to Boeing's baseline controller. Figure 3.11 compares the system response with the baseline controller and the $\mathcal{L}_1$ adaptive augmentation using a 4 rad/s) filter bandwidth, which achieves a 135 ms time delay margin. The virtual commands given by baseline controller and the $\mathcal{L}_1$ augmented controller are compared in Figure 3.12, along with their derivatives. It can be seen that the derivatives of the control signals with $\mathcal{L}_1$ and the baseline are very similar. It is important that the derivatives of the control action do not contain high frequencies, which may excite structural modes of an aircraft.

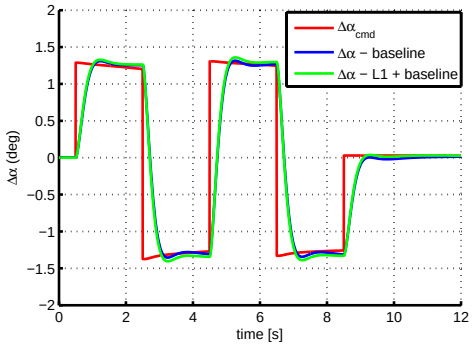

(a) AOA Tracking at Normal Flight AOA Trim

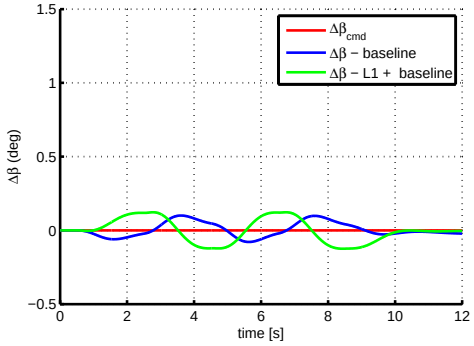

(b) Sideslip Maintenance at Normal Flight AOA Trim

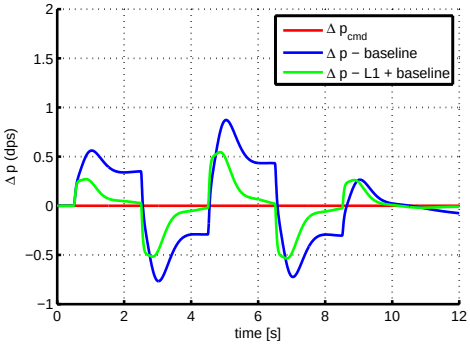

(c) Roll Rate Maintenance at Normal Flight AOA Trim

Figure 3.11: Pitch Command at Normal Flight AOA Trim with Reduced Bandwidth Filter

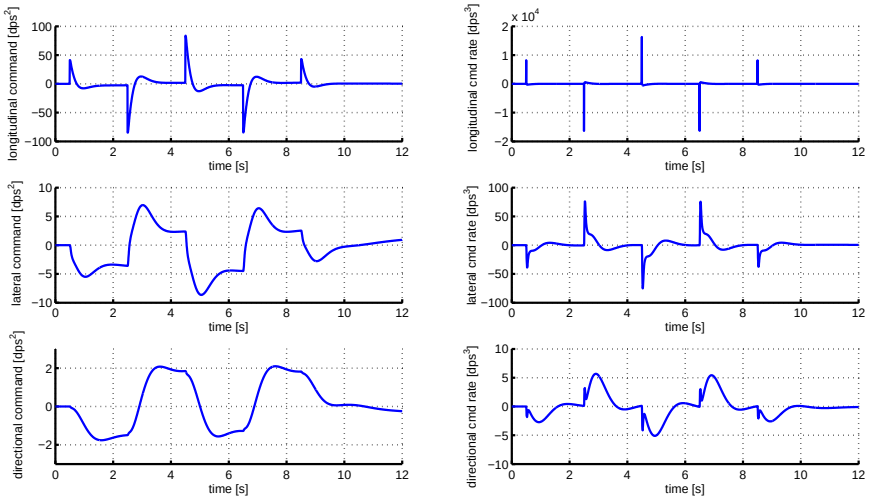

(a) Baseline Controller Commands and Derivatives

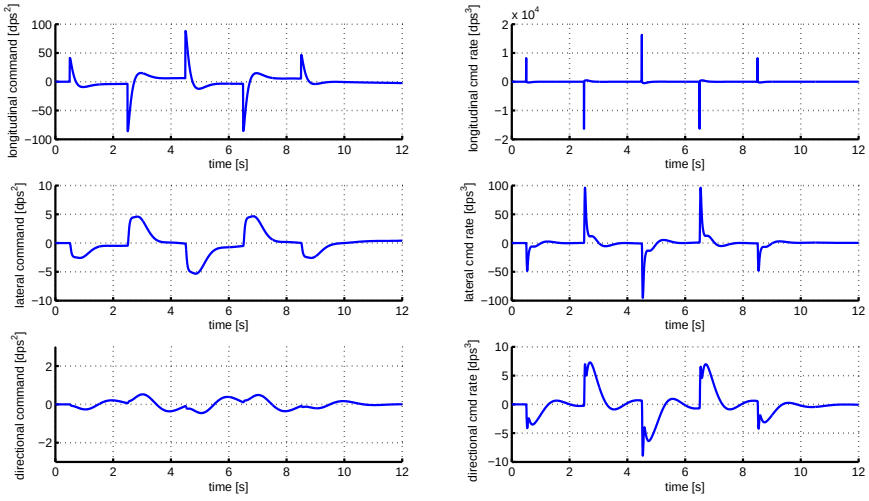

(b) $\mathcal{L}_1$ CAS Commands and Derivatives

Figure 3.12: Comparison of Virtual Pitch, Roll, and Yaw Acceleration Commands and Their Derivatives

Chapter 4

Conclusions and Future Work

An $\mathcal{L}_1$ adaptive control augmentation system that compensates for both matched and unmatched uncertainty has been presented for the X-48B Blended Wing Body. The $\mathcal{L}_1$ adaptive control theory was validated on a wide range of linear models of the X-48B in the presence of various failures. In these simulations, $\mathcal{L}_1$ adaptive augmentation demonstrates the potential for greatly improved performance for nominal flight conditions across the entire envelope with guaranteed robustness. In the event of a failure, the $\mathcal{L}_1$ adaptive controller adapts to recover desired aircraft performance and provide a predictable response to pilot inputs.

$\mathcal{L}_1$ theory has been extended to support input saturation constraints, such as control surface deflection limits. Control surface deflection and rate limits were not part of the X-48B models provided for this challenge problem. If higher fidelity models of the aircraft's dynamics could also be obtained,

the performance benefits of and $\mathcal{L}_1$ control augmentation system could be demonstrated in further detail. Future work could also include determining an appropriate minimum time delay margin for the X-48B models, tuning the filter to achieve this time delay margin, and analyzing the performance-robustness trade-off according to a true design requirement.

References

[1] Tyler Leman, Enric Xargay, Geir Dullerud, Naira Hovakimyan, and Thomas Wendel. $\mathcal{L}_1$ Adaptive Control Augmentation System for the X-48B Aircraft. In *AIAA Guidance, Navigation, and Control Conference*, Chicago, IL, August 2009.

[2] Jaiwon Shin. The NASA Aviation Safety Program: Overview. March 2000. NASA/TM2000-209810.

[3] Zhuquan Zang and Robert R. Bitmead. Transient Bounds for Adaptive Control Systems. In 30^{th} *IEEE Conference on Decision and Control*, pages 2724–2729, Brighton, U.K., December 1990.

[4] Chengyu Cao and Naira Hovakimyan. Design and Analysis of a Novel $\mathcal{L}_1$ Adaptive Control Architecture with Guaranteed Transient Performance. *IEEE Transactions on Automatic Control*, 53(3):586–591, 2008.

[5] Chengyu Cao and Naira Hovakimyan. Guaranteed Transient Performance with $\mathcal{L}_1$ Adaptive Controller for Systems with Unknown Time-Varying Parameters and Bounded Disturbances: Part I. In *Proc. of*

American Control Conference, pages 3925–3930, New York, NY, July 2007.

[6] Chengyu Cao and Naira Hovakimyan. Stability Margins of $\mathcal{L}_1$ Adaptive Controller: Part II. In *Proc. of American Control Conference*, pages 3931–3936, New York, NY, July 2007.

[7] Chengyu Cao and Naira Hovakimyan. $\mathcal{L}_1$ Adaptive Controller for a Class of Systems with Unknown Nonlinearities: Part I. In *Proc. of American Control Conference*, pages 4093–4098, Seattle, WA, June 2008.

[8] Isaac Kaminer, Oleg Yakimenko, Vladimir Dobrokhodov, Antonio Pascoal, Naira Hovakimyan, Chengyu Cao, Amanda Young, and Vijay V. Patel. Coordinated Path Following for Time-Critical Missions of Multiple UAVs via $\mathcal{L}_1$ Adaptive Output Feedback Controllers. In *AIAA Guidance, Navigation, and Control Conference*, Hilton Head Island, SC, August 2007.

[9] Chengyu Cao, Naira Hovakimyan, Isaac Kaminer, Vijay V. Patel, and Vladimir Dobrokhodov. Stabilization of Cascaded Systems via $\mathcal{L}_1$ Adaptive Controller with Application to a UAV Path Following Problem and Flight Test Results. In *American Control Conference*, New York, NY, July 2007.

[10] Randy W. Beard, Nathan B. Knoebel, Chengyu Cao, Naira Hovakimyan, and Joshua S. Matthews. An $\mathcal{L}_1$ Adaptive Pitch Controller

for Miniature Air Vehicles. In *AIAA Guidance, Navigation, and Control Conference*, Keystone, CO, August 2006.

[11] Jiang Wang, Vijay V. Patel, Chengyu Cao, Naira Hovakimyan, and Eugene Lavretsky. $\mathcal{L}_1$ Adaptive Controller for Tailless Unstable Aircraft in the presence of Unknown Actuator Failures. In *AIAA Guidance, Navigation, and Control Conference*, Hilton Head Island, SC, August 2007.

[12] Jiang Wang, Chengyu Cao, Vijay V. Patel, Naira Hovakimyan, and Eugene Lavretsky. $\mathcal{L}_1$ Adaptive Neural Network Controller for Autonomous Aerial Refueling with Guaranteed Transient Performance. In *AIAA Guidance, Navigation, and Control Conference*, Keystone, CO, August 2006.

[13] Jiang Wang, Vijay V. Patel, Chengyu Cao, Naira Hovakimyan, and Eugene Lavretsky. $\mathcal{L}_1$ Adaptive Neural Network Controller for Autonomous Aerial Refueling with Guaranteed Transient Performance. In *AIAA Guidance, Navigation, and Control Conference*, Keystone, CO, August 2006.

[14] Irene M. Gregory, Chengyu Cao, Vijay V. Patel, and Naira Hovakimyan. $\mathcal{L}_1$ Adaptive Control Laws for Flexible Semi-Span Wind Tunnel Model of High-Aspect Ratio Flying Wing. In *AIAA Guidance, Navigation, and Control Conference*, Hilton Head Island, SC, August 2007.

[15] Chengyu Cao, Naira Hovakimyan, and Eugene Lavretsky. Application of $\mathcal{L}_1$ Adaptive Controller to Wing Rock. In *AIAA Guidance, Navigation, and Control Conference*, Keystone, CO, August 2006.

[16] Yu Lei, Chengyu Cao, Eugene Cliff, Naira Hovakimyan, Andy Kurdila, Michael Bolender, and David Doman. Design of an $\mathcal{L}_1$ Adaptive Controller for an Air-Breathing Hypersonic Vehicle Model with Unmodelled Dynamics. In *AIAA Guidance, Navigation, and Control Conference*, Hilton Head Island, SC, August 2007.

[17] Irene M. Gregory, Chengyu Cao, Enric Xargay, Naira Hovakimyan, and Xiaotian Zou. $\mathcal{L}_1$ Adaptive Control Design for NASA AirSTAR Flight Test Vehicle. In *AIAA Guidance, Navigation, and Control Conference*, Chicago, IL, August 2009.

[18] NASA Dryden Flight Research Center. X-48B Blended Wing Body. Retrieved January 15, 2009 from http://www.nasa.gov/centers/dryden/research/X-48B/index.html.

[19] Enric Xargay, Chengyu Cao, and Naira Hovakimyan. $\mathcal{L}_1$ Adaptive Controller for Nonlinear Multi-Input Multi-Output Systems in the Presence of Significant Cross-Coupling. In *American Control Conference*, Baltimore, MD, June 2010.

[20] Dapeng Li, Naira Hovakimyan, Chengyu Cao, and Kevin A. Wise. Filter Design for Feedback-loop Trade-off of $\mathcal{L}_1$ Adaptive Controller: A Lin-

ear Matrix Inequality Approach. In *AIAA Guidance, Navigation, and Control Conference*, Honolulu, HI, August 2008.